CFD Investigation of The Hydrodynamic, Thermal, and Energy Characteristics of a Microchannel Biodiesel Reactor

[1]Nwakwuribe, V C; [2]Ugwu, H U; [2]Obi, A I
[1]Department of Mechanical Engineering,
Abia State University, Uturu, Abia State, Nigeria
[2]Department of Mechanical Engineering,
Michael Okpara University of Agriculture
Umudike, Abia State, Nigeria
[1]Corresponding Author Email:
chimaogevictor@gmail.com
[2]Co-Authors Email: ugwu.hyginus@mouau.edu.ng;
obi.anthony@mouau.edu.ng

https://doi.org/10.56201/ijemt.vol.12.no11.2026.pg24.38

Abstract
This study addresses the tendency of biodiesel reactor research to treat flow, heat transfer, and energetics separately, despite reactor efficiency depending on their coupled behaviour. Transient CFD simulations of an improved microchannel reactor were performed in ANSYS Fluent using a pressure-based coupled solver, with the methanol feed and oil introduced at 0.70 m/s and 1.20 m/s and inlet temperatures of 318 K and 333 K under laminar conditions (Re < 2300), after assessing mesh quality and confirming time-step independence. Results showed the combined velocity of the bio-oil and methanol feed streams after merging accelerated to 2.97 m/s within the microchannels tube, with slight recirculation in the settling chamber. Local pressure ranged from 3.7 to 11.3 kPa with an overall pressure drop of 2.56 kPa, while a thermal uniformity of 333 K was maintained within the reactors preheating chamber and microchannel tube. The Internal energy spanned from 53,530–59,890 J/kg in reactive zones but the lowest internal energy of −41,890 J/kg was recorded in the methanol feed inlet tube. Validation against experimental data gave errors of 2.69% (temperature), 2.66% (pressure drop), 2.62% (velocity), and 1.60% (Biodiesel yield), all within the 5% threshold. The results demonstrate the applicability of the CFD framework to the investigated microreactor configuration and provide a basis for further design optimization and scale-up studies.

Keywords
Biodiesel production, Microchannel reactor, Computational fluid dynamics (CFD), ANSYS Fluent simulation

1.0 Introduction

Renewable energy remains a defining challenge for 21st-century engineering because fossil fuels are finite, volatile in price, and polluting. A promising alternative to this is the use of biodiesel produced from waste oils and lipids, which can help reduce greenhouse gas (GHG) emissions and the dependence on fossil fuels (Farouk *et al*., 2024; Osman *et al*., 2024). However, its production is contingent upon the efficiency of the transesterification step, in

which the catalyst type, feedstock, and process conditions collectively determine conversion, cost, and environmental performance (Awogbemi *et al*., 2024; Farouk *et al*., 2024). Therefore, the commercial viability of biodiesel is centred on the development of more efficient reactor technologies that should lead to reduced energy consumption, reduced processing time and improved fuel quality (Farouk *et al*., 2024; Osman *et al*., 2024). More recently, microchannel reactors have gained a lot of attention due to their better heat and mass transfer, quicker mixing and ability for small-scale continuous operation in contrast with large stirred tanks (Huchet, 2011; Majnis & Jalwan, 2019). Due to internal circulation and internal contact, which is better than stratified flows, the alcohol and oil form slug or droplet flows, which are considered advantageous for the ester yield (Horta *et al*., 2014; Kushaari *et al*., 2019; Laziz *et al*., 2019). This complexity made Computational Fluid Dynamics (CFD) a necessary tool to understand the flow variables that are difficult to measure experimentally like velocity, pressure and thermal field (Osman *et al*., 2024; Sandoval *et al*., 2016), and its validation was tested against benchmark data by employing either the finite volume scheme or the lattice Boltzmann scheme (Kadivar *et al*., 2022; Widyaparaga & Pranowo, 2013) or both. The literature of microchannel heat exchangers shows that the geometry plays a major role in determining the pressure drop and heat transfer characteristics (Meral & Parlak, 2021). Despite these advances, the literature is fragmented: reviews discuss feedstocks, catalysts and economics without spatially resolved transport data (Meral & Parlak, 2021; Rohaizan *et al*., 2024) catalyst studies neglect reactor conditions (Awogbemi *et al*., 2024); flow simulations often mis-predict regimes observed experimentally (Laziz *et al*., 2019); interface-focused multiphase studies neglect energy balances (Horta *et al*., 2014); and advances in reactor-scale CFD remain restricted to macro-scale systems (Du *et al*., 2022). In spite of the achievements in the microchannel reactor designs, very few attempts have been made to provide an integrated flow, heat and energy picture. The performance of many of these designs in terms of uneven flow, pressure loss, improper mixing, and uneven heat is still very unsatisfactory. Consequently, the application of these microchannel reactors to industrial production on a large scale is hindered (Huchet, 2011; Osman *et al*., 2024). The present study addresses this gap, flow velocity, pressure, temperature and internal energy are mutually related within a micro-channel because if one variable rises, the other concurrently escalates adversely unless their interconnectedness is examined within a unified framework. For instance, narrowing a microchannel in order to facilitate proper mixing will increase either the frictional resistance in the channel or will generate some thermal unevenness somewhere along the channel (Meral & Parlak, 2021; Ren *et al*., 2025). In the present work, the effects of hydrodynamic, thermal and energy behaviours on the improved microchannel biodiesel reactor were considered. These characteristics of the improved reactor have been simulated using CFD. The principal objectives of the present work are: 1) to analyse the velocity contours across the channel in order to study flow regime; 2) to determine and analyse pressure drops across the channel to consider the frictional penalty resulting from the new configuration; 3) to analyse temperature fields, focusing on temperature distribution along the walls and across the channel in relation to wall conduction and flow behavior in the improved microchannel. 4) to calculate the internal energy in the system so as to link the flow pattern with the thermal field and achieve a better understanding of the behavior of energy in the fluid. The novelty of this work lies in the coupled analysis of flow, heat transfer and energy that has rarely been investigated for biodiesel reactors in the micro-scale dimensions, although it has already been studied for heat exchangers and microchannel heat sinks and flow boiling (Meral & Parlak, 2021; Odumosu *et al*., 2024). The results provide useful information for subsequent reactor optimization and future scale-up or numbering-up investigations.

2.0 Materials and Methods

The materials used in this study are heating elements, mild steel plates and angle iron, k type thermocouple temperature sensors, digital temperature and differential pressure transducers, a microchannel tube comprising of interconnected helical microchannels with a single inlet for the bio-oil and methanol feed (methanol + dissolved NaOH catalyst) fabricated using SS304 stainless steel capillary tubing with an outer diameter of 1.6 mm and an inner diameter of 0.8 mm, 12.7 mm inner diameter stainless steel pipes, the inlet tubes for the preheated bio-oil and methanol feed were made using SS304 stainless steel capillary tubing with an outer diameter of 1.6 mm and an inner diameter of 1 mm, 12.7 mm inner diameter stainless steel pipe fittings, flow control valves, temperature controllers, electric wires, bolts and nuts, SOLIDWORKS, Autodesk Inventor Professional 2024 and ANSYS Fluent software.

2.1 Biodiesel Reactor Design Considerations, Concept, and Configuration

The successful conversion of feedstock in a biodiesel reactor requires a delicate balance of chemical kinetics, optimal mass transfer, and precise heat control. This section discusses the important technical principles and structural designs necessary for properly scaling the transesterification process. The framework provides the basis for developing a secure, high-yield, commercially feasible biodiesel production system by analysing key setup parameters. The reactor concept view is shown in figure 1 below.

2.2 Design Considerations for Biodiesel Reactor

In designing the reactor, the following factors were taken into account, to make it as efficient and reliable as possible:

a) The machine should be of a considerable capacity and able to reduce the demand for labour.
b) The reactor should be portable and easy to operate. It should be made in a way that it is able to process different types of feedstock.
c) The materials used should be readily available and preferably sourced locally;
d) The construction materials should not contaminate the biodiesel produced and should be resistant to chemicals, corrosion and wear.
e) The overall cost of the reactor should be affordable and available to anyone wishing to produce biodiesel.

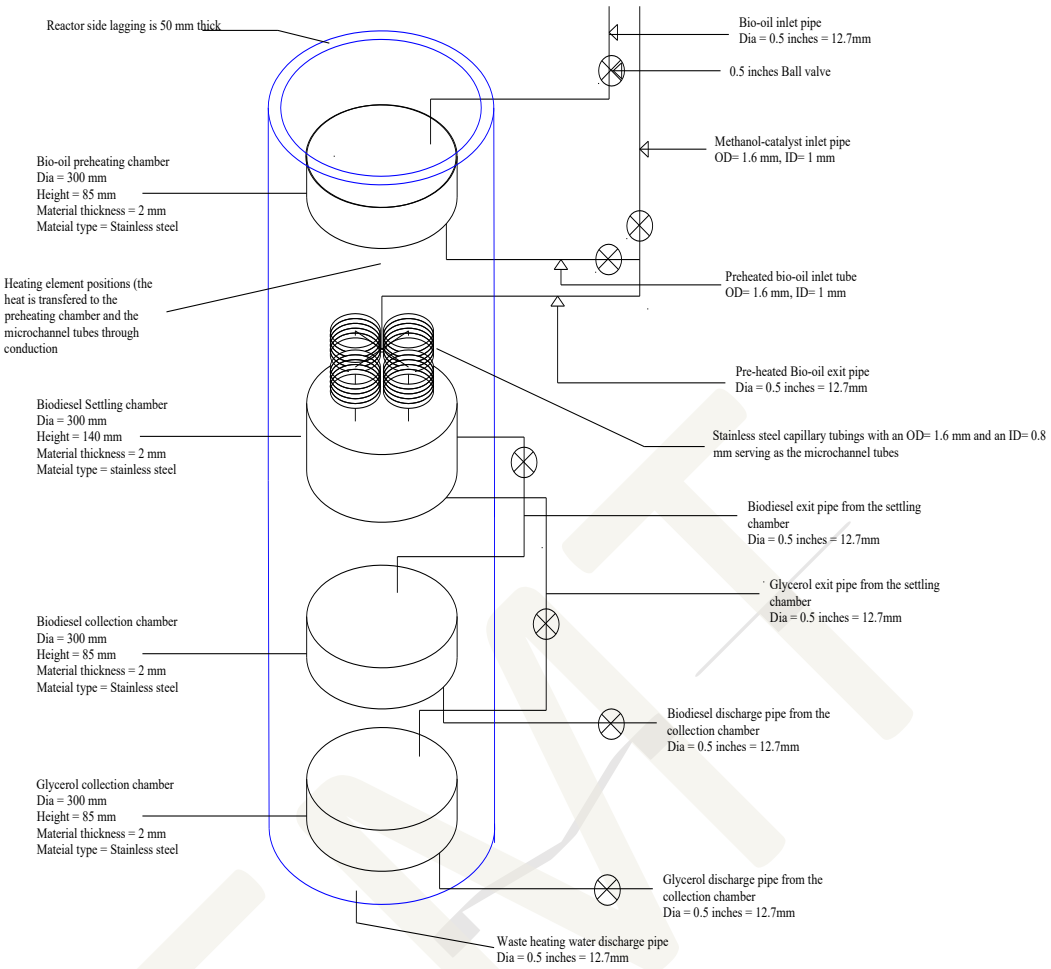


Figure 1: Detailed design concept of the microchannel biodiesel reactor

2.3 Brief Description of the Concept Biodiesel Reactor Operation Principle

The bio-oil is introduced into the reactor through the bio-oil intake pipe and conveyed to the pre-heating chamber, where it is heated to the desired reaction temperature by an electric heating element. This pre-heating stage is essential for reducing the viscosity of the bio-oil, improving its miscibility with the methanol feed, and providing sufficient thermal energy to overcome the activation energy required for the transesterification reaction. Consequently, the reactants achieve improved reaction kinetics and higher conversion efficiency.

The preheated bio-oil is subsequently combined with the methanol feed before entering the microchannel tube network. Within the microchannels, the reactants undergo intensive mixing and efficient heat transfer, facilitated by the high surface-area-to-volume ratio of the channels. This enhanced mass and heat transfer promotes the continuous transesterification of triglycerides into fatty acid methyl esters (biodiesel) and glycerol. The reaction mixture then flows into the storage and collection chambers for subsequent phase separation and product recovery.

2.4 Analysis of microchannel biodiesel reactor performance by computational fluid dynamics

The model configuration was adopted from the two-dimensional reactor geometry designed in SolidWorks, and the meshed domain was exported for pre-processing and numerical analysis.

The simulation was initiated by importing the CAD model developed in Autodesk Inventor Professional 2024 into ANSYS Workbench.

2.5 Assumptions for the Numerical Model

The following assumptions are made to simplify the numerical modelling and to increase computational efficiency.

a) The reactor geometry is assumed to conform exactly to the CAD design, with no manufacturing defects, dimensional deviations, or surface irregularities that could influence the flow characteristics.

b) The reactor is assumed to approach a quasi-steady operating condition, with laminar flow (Re < 2300) prevailing throughout the microchannel under normal operating conditions. A transient solver was employed for the numerical simulations, and the solution was allowed to evolve until outputs stabilized within an acceptable tolerance (see Section 2.7).

c) The flow is assumed to be incompressible and at a low Mach number (Ma < 0.3) since both the methanol feed and the oil are liquids.

d) The influence of the forces of gravity on the flow field is neglected due to the small sizes of the channels and the horizontal position of the reactor.

e) Heat losses to the environment are negligible unless otherwise stated. The baseline scenario assumes adiabatic walls but some scenarios include a steady heat flux to simulate the heating jacket.

f) The process follows a first or pseudo-first order kinetic model for the concentration of triglycerides assuming an excess of methanol feed

g) Mass transfer limitations between the methanol feed and oil phase are neglected and perfect miscibility is achieved in the microchannel due to vigorous mixing.

h) The physical parameters of the reacting mixture are approximated by those of a binary liquid mixture (methanol feed and oil) and updated with temperature, but not with conversion.

2.6 Mathematical Modelling of Conservation Equations

The flow dynamics, thermal transfer and reaction kinetics in the microchannel biodiesel reactor were modelled by means of Computational Fluid Dynamics (CFD). CFD simulations were performed with ANSYS Fluent, a commercial software that solves the governing conservation equations of mass, momentum, energy and species movement in three dimensions. The governing equations below include continuity, momentum (Navier–Stokes), energy and species movement. The chemical kinetics of the transesterification reaction were incorporated to properly describe the dynamics of biodiesel production.

2.6.1 The continuity equation

Equation 1 is the continuity equation which guarantees the conservation of mass in the flow domain.

$$\nabla \cdot (\rho \boldsymbol{v}) = 0 \quad (1)$$

Where (ρ) = fluid density (kg/m³), $(\boldsymbol{v}) = velocityvector(m/s)$.

2.6.2 The momentum equation (Navier–Stokes equation)

The momentum equation that indicates conservation of linear momentum was formulated to study the conservation of linear momentum in the reacting fluid in the reactor. Here, forced convection is taking place inside a horizontal microchannel in the reactor, and the effect of body forces (such as gravity) is negligible and thus not considered. The forces considered for driving and resisting are pressure and viscous forces respectively which are responsible for

velocity distribution in the reactor. Equation 2 is the momentum equation describing the conservation of linear momentum in the fluid.

$$\rho\left(\frac{\partial v}{\partial t} + v \cdot \nabla v\right) = -\nabla p + \mu \nabla^2 v \quad (2)$$

Where (p) = static pressure (Pa), (μ) = dynamic viscosity (Pa·s). This equation captures the velocity field development within the microchannels and accounts for viscous and pressure effects influencing flow stability.

2.6.3 The energy equation

Equation 3 is the energy equation which shows heat transfer due to conduction, convection and viscous dissipation in the reacting flow.

$$\rho C_p\left(\frac{\partial T}{\partial t} + v \cdot \nabla T\right) = \nabla \cdot (k \nabla T) + S_T \quad (3)$$

Where (C_p) = specific heat capacity (J/kg·K), (T) = temperature (K), (k) = thermal conductivity (W/m·K), (S_T) = source term representing heat generated or absorbed during the chemical reaction. This formulation allows accurate prediction of temperature distribution along the microchannel reactor length.

2.6.4 The equation for species transport

Species conservation equation describes the movement of chemical species (oil, methanol feed and products) in the reactor. As seen in equation 4.

$$\frac{\partial(\rho Y_i)}{\partial t} + \nabla \cdot (\rho \boldsymbol{v} Y_i) = -\nabla \cdot \boldsymbol{J_i} + R_i \quad (4)$$

Where (Y_i) = mass fraction of species *i*, $(\boldsymbol{J_i})$ = diffusion flux of species *i*, (R_i) = rate of production or consumption of species *i* due to chemical reactions. This equation was solved for all species involved in the transesterification process, ensuring accurate modelling of concentration gradients along the microchannel.

2.6.5 Chemical kinetics model

The transesterification of triglycerides with methanol feed was simulated as a reversible three-step reaction catalysed by NaOH. The universal kinetic equation is given by equation 5.

$$r = k \prod C_i^{n_i} \quad (5)$$

Where (r) = reaction rate (mol/m³·s), (k) = rate constant (temperature-dependent via Arrhenius relation), (C_i) = concentration of reactant *i*, (n_i) = reaction order for species *i*. The kinetic parameters were obtained from published literature and applied to the present operating conditions without fitting to the experimental results used for model validation**.** The product operator ($\prod$) is analogous to the summation operator (Σ), but instead of summing, it multiplies a series of terms together. For a reaction involving three reactants, it would expand to equation 6.

$$r = k C_A^{n_A} C_B^{n_B} C_C^{n_C} \quad (6)$$

2.6.6 Flow and turbulence modelling characterisation

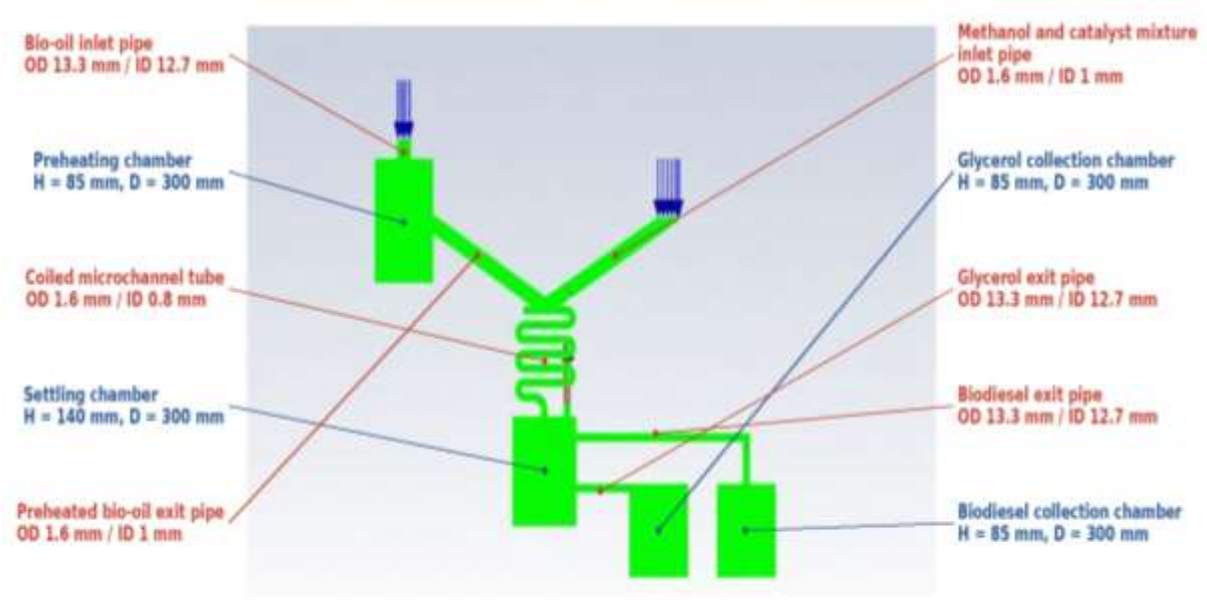
The flow behaviour in the microchannel was characterised by the Reynolds number (Re) as given by the equation 7.

$$Re = \frac{\rho u D}{\mu} \quad (7)$$

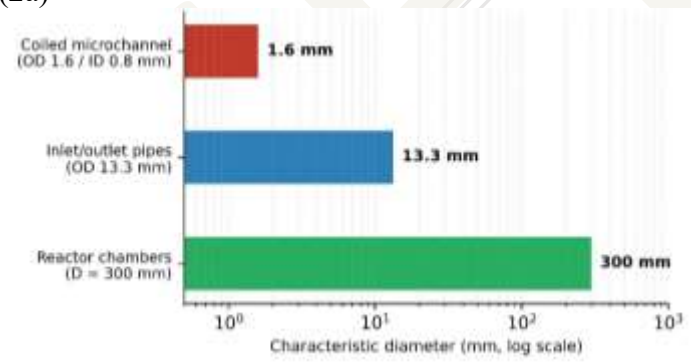
Where (u) = average velocity (m/s), (D) = hydraulic diameter (m).

2.7 Computational Fluid Dynamics Setup

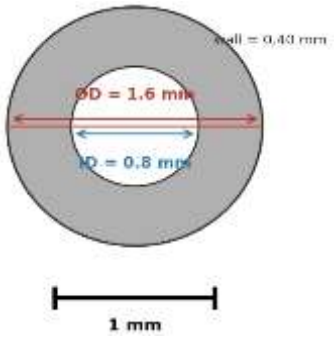
The governing equations of mass, momentum, energy and species transport were solved using pressure based transient solver. The evolution of the reacting flow was tracked until a quasi-steady solution was reached using the transient formulation. The species transport was modelled with volumetric reactions activated and the energy equation was adjusted to account for the temperature variation during the reaction. Coupled scheme was used for pressure-velocity coupling to obtain stable results in the lminar reacting flow. The second-order upwind methods were used for momentum, energy and species to preserve the accuracy of the results. Published data treated properties like density, viscosity, heat capacity and thermal conductivity to be temperature dependent. The computational geometry of the microchannel biodiesel reactor used for the CFD simulations is shown in figure 2a.



(2a)



(2b)



(2c)

Figure 2a: Computational geometry of the microchannel biodiesel reactor used for the CFD simulations. Components are shown schematically and are not rendered to a single common scale; the coiled microchannel (OD = 1.6 mm) is drawn larger than its true proportion relative to the chambers (D = 300 mm) preheated oil, methanol feed inlet tubes (OD= 1.6 mm) and connecting pipes (OD = 13.3 mm) for visibility, (2b) compares the true relative scale of the reactor components, while (2c) shows the microchannel tube cross-section drawn to its own true scale with a 1 mm scale bar.

The inlet boundary conditions were specified based on the experimental operating conditions. The methanol feed was introduced into the reactor at 318 K with an inlet velocity of 0.70 m/s,

whereas the oil feed (waste cooking oil) was supplied at 333 K and an inlet velocity of 1.20 m/s. Each inlet was of pure composition with the catalyst added as an additional species where relevant. The system was operated at 1 bar, with the outlet at 0 Pa gauge pressure and no-slip conditions were assigned to the solid walls. Two wall conditions were investigated: no heat loss, and a fixed heat flux to represent a heating jacket. For the results presented in Sections 3.2 – 3.7 and the subsequent validation against experimental measurements, the fixed-heat-flux wall condition was adopted to represent the heat supplied by the reactor heating system. The adiabatic-wall condition was used only as a reference case for assessing the influence of external heat transfer. Time stepping was performed at 0.01 s intervals for 10,000 steps, for a total simulated time of 100 seconds with up to 50 iterations per time step. Convergence required strict residual limits and mass balance checks and results were considered stable when key outputs changed by less than 2% through the steps. The simulations were started from the same initial conditions, occasionally with ramp-up of inputs to prevent shocks. The data were saved at intervals for the later analysis of velocity, temperature, species and pressure.
Sensitivity checks confirmed the robustness of the results. The results were consistent for different time steps. Turbulence models were attempted but showed little difference from the laminar model, confirming the laminar flow was the correct choice.

2.8 Computational Mesh Generation and Quality Assessment

The geometry of the reactor was meshed with ANSYS Meshing (Fluent CFD Prep-Post) using an unstructured triangular mesh, as shown in Figure 3. This meshing approach allowed flexibility in handling the complex geometry, particularly in the curved and constricted regions such as the coiled microchannel and the inlet junctions. Given the large disparity in scale between the reactor chambers and connecting pipes on one hand, and the 0.8 mm ID microchannel tube on the other, a two-tier sizing strategy was adopted. A global element size of 1200 µm was applied to the reactor chambers and connecting pipes, while a local body sizing control of 32 µm was applied to the microchannel and inlet regions, corresponding to a nominal resolution of approximately 25 elements across the channel diameter. This local refinement was necessary to adequately resolve the velocity, thermal, and species gradients described in Section 2.6, which would not have been captured by the coarser global sizing alone. Mesh de-featuring and curvature capture were additionally used to improve surface resolution and preserve geometric accuracy in the curved sections of the microchannel.
The mesh was checked with three standard quality metrics. Orthogonal quality ran from 0.74216 to 1.00000, averaging 0.96245. Skewness stayed between 0.15 and 0.46, with a mean of 0.27. Aspect ratio spanned 1.60 to 4.20 (mean 3.10), so no triangle is stretched beyond about four to one. Even the worst cells sat inside the ranges the solver documentation recommended.

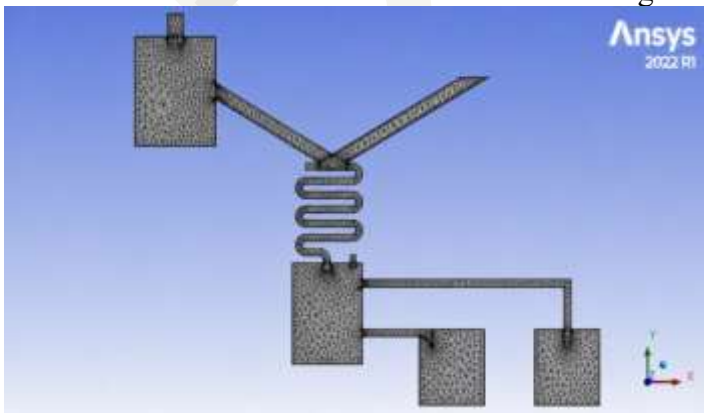


Figure 3: Computational mesh generated for the microchannel biodiesel reactor. As in Figure 2, components are shown schematically and are not rendered to a single common scale

2.9 Time Step Independence

A time-step independence test was also carried out to confirm the accuracy and numerical stability of the transient CFD simulations. The influence of three different time steps, 0.005 s, 0.01 s and 0.02 s, on solution convergence, stability and computational efficiency were investigated. The analysis was performed to identify an adequately small-time increment that would enable precise modelling of transient changes in velocity, temperature and species concentration without numerical instability or excessive computational cost. Simulations were run for each time step for uniform operating conditions. The main variables monitored were the output average velocity, the average reactor temperature and the biodiesel mass fraction. The results showed that the smaller time step (Δt = 0.005 s) gave very accurate results, but required a much higher number of repetitions and computational time. The larger time step (Δt = 0.02 s) accelerates the calculations, but it leads to significant numerical oscillations and prevents convergence, particularly for the energy and species transport equations. The intermediate time step (Δt = 0.01 s) provides the best trade-off between accuracy and processing efficiency. The predicted velocity and temperature profiles showed a divergence less than 1.5% when compared to the finer time step (Δt = 0.005 s), while maintaining smooth residual convergence and stable temporal behaviour. Figure 4 illustrates the convergence of the solution in relation to time.

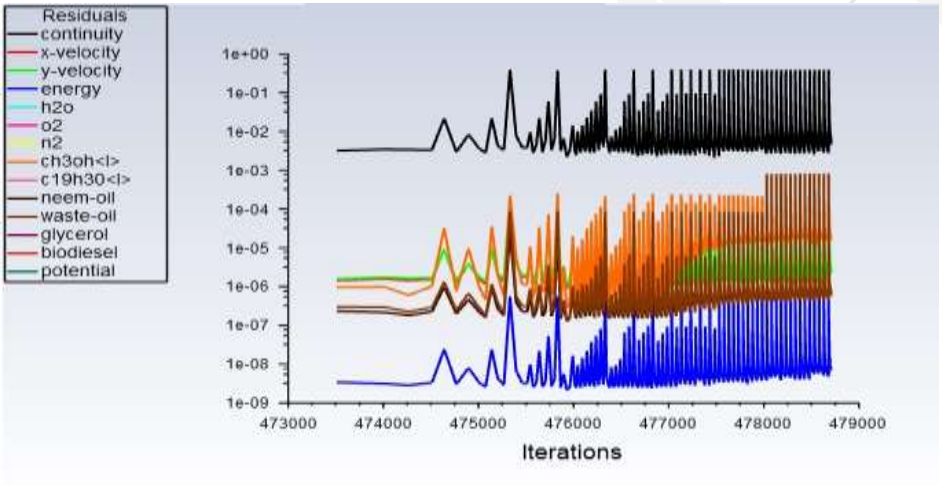


Figure 4: Effect of time-step size on the convergence of the transient CFD solution.

3.0 Results and Discussion

3.1 Numerical Evaluation of the Reactor Performance

The computational grid and the time parameters were verified and the reactor performance was evaluated numerically. In this study, the interaction of fluid mechanics and thermal transport in the microchannel tubes was investigated. To measure the efficiency of the reactant mixing and thermal energy transfer the internal flow dynamics were assessed. The observed hydrodynamic behaviour is described in the following sections, including the velocity, and pressure profiles, together with the resulting thermal and internal energy distribution. The combined profiles allow a complete evaluation of the operational performance of the reactor and also reveal critical factors that influence the biodiesel conversion process.

3.2 Analysis of the Flow Field in the Biodiesel Reactor

The entrance velocities of methanol feed and oil are 0.7 m/s and 1.2 m/s respectively for adequate mixing without losing laminar flow in the microchannel. The feed temperatures of 318 K for the methanol feed, and 333 K for oil were used to demonstrate the warmed feed

conditions that optimise transesterification kinetics. The simulation results show that the average pressure drop is about 2.56 kPa, indicating that the flow is effective and the hydraulic resistance is small. Table 1 shows the main input and output parameters used in the CFD simulation of the microchannel biodiesel reactor.

Table 1: Summary of key simulation parameters

S/No	Parameter	Value
1	Inlet Velocity (Methanol feed)	0.7 m/s
2	Inlet Velocity (Oil)	1.2 m/s
3	Inlet Temperature (Methanol feed)	318 K
4	Inlet Temperature (Oil)	333 K
5	Pressure Drop	2.56×10^{3} Pa

3.3 Distribution of Velocity Contours in the Biodiesel Reactor

The CFD simulation of the biodiesel reactor revealed different velocity regions. Bio-oil was fed at 1.2 m/s and methanol feed at 0.7 m/s. The two streams were mixed in a microchannel tube with the diameter of 0.8 mm and the velocity increased to approximately 2.97 m/s according to the principle of mass conservation. The velocity increase was caused by the decrease in tube diameter from 1.0 mm to 0.8 mm. The microchannel exhibited the highest velocity magnitudes, with relatively uniform bulk velocity along the channel, while the curved geometry generated secondary vortical structures that promoted convective mixing. The velocity decreased substantially downstream in the settling chamber, where localized recirculation was observed before the product entered the collection stage. Therefore, the microchannel was the high-velocity core of the reactor.

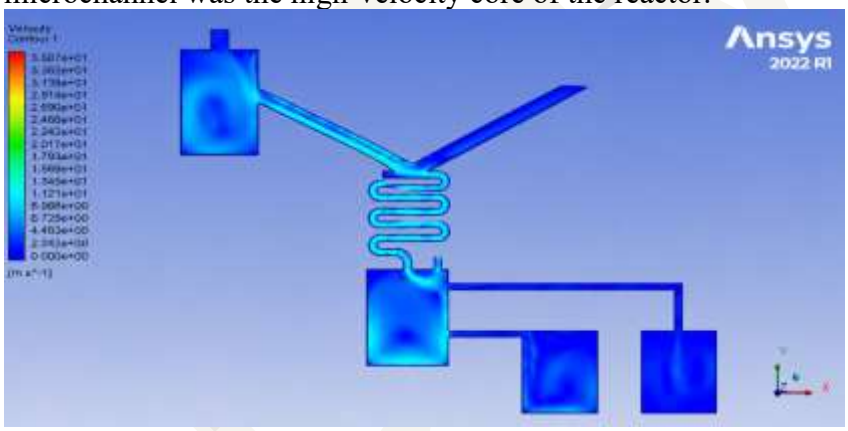


Figure 5: Velocity magnitude distribution within the biodiesel reactor.

3.4 Pressure Distribution in the Biodiesel Reactor

Figure 6 shows the spatial distribution of local gauge pressure in the reactor at the range of 3.7 to 11.3 kPa with the total pressure drop of about 2.56 kPa from inlet to outlet. The reported local pressure range (3.7–11.3 kPa) reflects gauge pressure within the interior flow domain as visualized in Figure 6; values approach the fixed 0 Pa gauge condition at the outlet boundary itself, which lies outside the plotted contour range. This implies a low hydraulic resistance and a fairly uniform pressure field. The preheating chamber, microchannel tubes and settling chamber show similar pressure levels, implying small gradients resulting from low flow activity. The lack of large high- or low-pressure areas means the pressure distribution is stable which is good for structural integrity and uniformity of reactor performance.

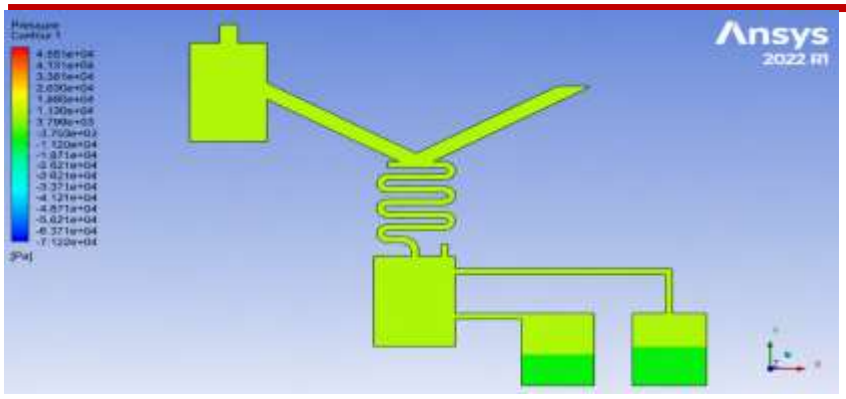


Figure 6: Static pressure distribution within the biodiesel reactor.

3.5 Temperature Distribution in the Biodiesel Reactor

As shown in Figure 7 the reactor maintained a high temperature throughout the process. The pre-heated bio-oil and methanol feed were fed at 333 K and 318 K, respectively. The preheating chamber and the microchannel tube were dominantly at a temperature of about 333 K, while the methanol feed inlet was cooler at 318 K. The microchannel temperatures were uniform with slight decrease in the discharge section. Overall, this showed an effective thermal mixing and retention of heat, with the only non-uniformity in temperature at the inlet stage prior to homogenisation.

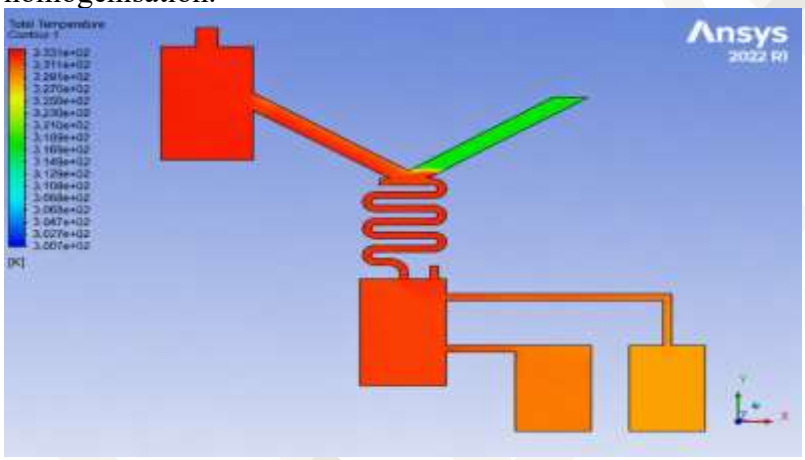


Figure 7: Total temperature distribution within the biodiesel reactor.

It should be noted that the 333 K uniformity described here refers to the dominant temperature within the microchannel and preheating chamber specifically, whereas the average reactor temperature reported in Table 2 (326 K) is a domain-wide spatial average that includes the cooler 318 K methanol feed inlet region prior to mixing. This distinction accounts for the difference between the locally uniform 333 K core and the lower whole-domain average used for experimental validation.

3.6 Internal Energy Distribution in the Biodiesel Reactor

The internal energy contour (Figure 8) showed a large energy gradient within the reactor. The preheating chamber, microchannel tubes and settling chamber were marked with dark red shading, which corresponded to high internal energy values in the range of 53,530–59,890 J/kg. Conversely, the methanol feed inlet section showed a distinct blue colour, suggesting a much lower range of internal energy from −41,890 to −16,450 J/kg. Thus, the methanol feed stream had substantially less thermal and kinetic energy than the preheated bio-oil before they met at the entrance of the microchannel tube. It is important to point out that the reported internal

energy values are relative to the thermodynamic reference state as defined in the CFD material property settings. Therefore, the negative values at the methanol feed inlet should not be interpreted as negative energy in an absolute physical sense, but rather as a lower energy content in relation to the selected reference state. This is a standard practice adopted by CFD solvers to enable the comparison of thermal energy content of different fluid regions within the reactor. The fluid maintained high internal energy levels (53,530–59,890 J/kg) as it passed through the microchannel tubes and these levels gradually decreased downstream. The discharge chamber showed mid-range green/cyan values (9,999–21,720 J/kg) which further fell to blue tones (−22,810 to −35,530 J/kg) indicating a reduction in the local specific internal energy as the fluid passed through the downstream collection stages.

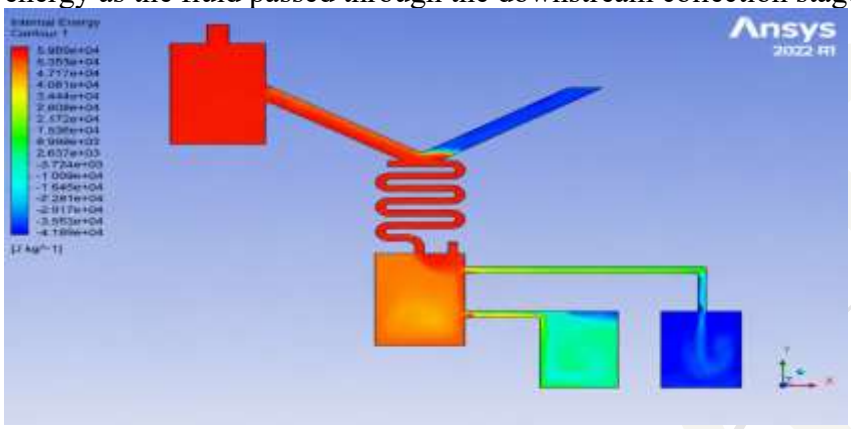


Figure 8: Specific internal energy distribution within the biodiesel reactor.

3.7 Validation of CFD Model Using Experimental Data

Experimental investigations were performed under the same operating conditions as the numerical simulations in an effort to evaluate the predictive capability of the developed computational fluid dynamics (CFD) model. The validation was carried out using experimentally measurable reactor performance parameters such as average reactor temperature, average reactor velocity, pressure drop and biodiesel yield. These parameters were chosen because they directly influence the hydrodynamic and thermal behaviour of the reactor and are commonly reported in CFD validation studies of continuous-flow biodiesel reactors. The reactor was operated at inlet velocities of 0.70 m/s for the methanol feed stream and 1.20 m/s for the oil stream. The inlet temperatures were kept at 318 K and 333 K respectively. The temperature of the reactor was measured by calibrated Type-K thermocouples located at strategic locations along the reactor and the pressure drop across the reactor was measured by differential pressure transducers located at the inlet and outlet. After the transesterification process was completed, the biodiesel yield was calculated gravimetrically and the biodiesel product was purified and dried.

The percentage error between the numerical predictions and the experimental measurements was calculated by using Equation 8.

$$\%\,age\ error = \frac{Measured\ Experimental\ Data - CFD\ data}{Measured\ Experimental\ Data}\ x\ 100 \qquad (8)$$

The results of the validation study are presented in Table 2.

Table 2: Comparison of CFD predictions with experimental measurement

Parameter	CFD Prediction	Experimental Result	Percentage Error (%)
Average reactor temperature (K)	326	335	2.69
Pressure drop (Pa)	2560	2630	2.66

Average Velocity in Microchannel (m/s)	2.97	3.05	2.62
Biodiesel yield (%)	92.5	94	1.60

The percentage error for each parameter was calculated as follows.
Average temperature

$$\%\, age\ error = \frac{335 - 326}{335}\ x\ 100 = 2.69 \quad (9)$$

Pressure Drop

$$\%\, age\ error = \frac{2630 - 2560}{2630}\ x\ 100 = 2.66 \quad (10)$$

Average velocity

$$\%\, age\ error = \frac{3.05 - 2.97}{3.05}\ x\ 100 = 2.62 \quad (11)$$

Biodiesel yield

$$\%\, age\ error = \frac{94 - 92.5}{94}\ x\ 100 = 1.60 \quad (12)$$

The validation results indicate good agreement between the numerical predictions and experimental measurements, with percentage errors ranging from 1.60% to 2.69%. These relatively small differences indicate that the CFD model adequately reproduces the experimentally measured temperature, pressure drop, velocity and biodiesel yield under the investigated operating conditions. Minor differences obtained from the numerical simulation when compared to experiments can be explained due to unavoidable experimental errors (e.g. Measurement uncertainties due to sensors precision and accuracy, slight change of inlet parameters and feedstock characteristics), simplifications imposed in the numerical model (e.g. Uniform material properties, idealized boundary conditions and neglect of heat transfer to the ambient) . Overall, there is good agreement, proving that the constructed CFD model is sufficiently accurate to predict the hydrodynamic and thermal performance of the microchannel biodiesel reactor and can be applied for investigation of reactor behavior, design optimization, scale-up studies, etc.

4.0 Conclusion

The study employed a validated coupled CFD framework to quantify the hydrodynamic, thermal and energy performance of an improved microchannel biodiesel reactor. The reactor maintained a low overall pressure drop (2.56 kPa) even at high in-channel velocity of 2.97 m/s, thermal uniformity 333 K across the reaction core and a slight chamber-level circulation that enhances interfacial mixing without compromising flow stability. The analysis of the internal energy showed that the highest specific internal-energy regions were concentrated in the preheating chamber, microchannel tubes, settling chamber with the lowest internal energy value observed in the methanol feed inlet tube. The errors are in the range of 1.60 – 2.69% for temperature, pressure drop, velocity and biodiesel yield when validated with experimental data which shows the predictive reliability of the model.
These results demonstrate that the coupled hydrodynamic, thermal and energy behaviour of the microchannel geometry can be evaluated within an integrated CFD framework, providing a quantitative basis for further reactor design, optimization, future scale-up or numbering-up studies.

References

Awogbemi, O., Ojo, A. A., & Adeleye, S. A. (2024). Advancements in the application of metal oxide nanocatalysts for sustainable biodiesel production. *Discover Applied Sciences*, *6*(5). https://doi.org/10.1007/s42452-024-05920-3

Du, X., Liu, M., & Sun, Y. (2022). Optimization of the internal circulating fluidized bed using computational fluid dynamics technology. *Fluid Dynamics & Materials Processing*, *18*(2), 303–312. https://doi.org/10.32604/fdmp.2022.016242

Farouk, S. M., Tayeb, A. M., Abdel-Hamid, S. M. S., & Osman, R. M. (2024). Recent advances in transesterification for sustainable biodiesel production, challenges, and prospects: A comprehensive review. *Environmental Science and Pollution Research*, *31*(9), 12722–12747. https://doi.org/10.1007/s11356-024-32027-4

Horta, A. A., Ferreira, L. O. S., Martinez, E. L., & Filho, R. M. (2014). Simulation of the alcohol-oil mixture in a T-shaped microchannel using the dissipative particle dynamics method on GPU devices. *Revista de Engenharia Térmica*, *13*(1), 65. https://doi.org/10.5380/reterm.v13i1.62072

Huchet, F. (2011). Flow and mass transfer inside networks of minichannels. In *InTech eBooks*. https://doi.org/10.5772/15272

Kadivar, M., Tormey, D., & McGranaghan, G. (2022). CFD of roughness effects on laminar heat transfer applied to additive manufactured minichannels. *Heat and Mass Transfer*, *60*(12), 1915–1929. https://doi.org/10.1007/s00231-022-03268-1

Kushaari, K., Laziz, A. M., & Hamid, N. H. (2019). Quantitative analysis of interfacial area on liquid-liquid multiphase flow of transesterification process in cross-junction microchannel reactor. *Journal of Engineering and Technological Sciences*, *51*(4), 585–596. https://doi.org/10.5614/j.eng.technol.sci.2019.51.4.9

Laziz, A. M., Kushaari, K., Chin, J., & Denecke, J. (2019). Quantitative analysis of hydrodynamic effect on transesterification process in T-junction microchannel reactor system. *Chemical Engineering and Processing: Process Intensification*, *140*, 91–99. https://doi.org/10.1016/j.cep.2019.04.019

Majnis, M. F., & Jalwan, M. R. (2019). Numerical investigation on multiphase flows in various configurations of microchannels using computational fluid dynamics. *ASEAN Journal of Chemical Engineering*, *17*(1), 82. https://doi.org/10.22146/ajche.49568

Meral, Z. K., & Parlak, N. (2021). Experimental research and CFD simulation of cross flow microchannel heat exchanger. *Journal of Thermal Engineering*, *7*(2), 270–283. https://doi.org/10.18186/thermal.872366

Odumosu, O. A., Li, H., Wang, T., & Che, Z. (2024). Conjugate heat transfer effects on bubble growth during flow boiling heat transfer in microchannels. *Physics of Fluids*, *36*(12). https://doi.org/10.1063/5.0242693

Osman, A. I., Nasr, M., Farghali, M., Rashwan, A. K., Abdelkader, A., Al-Muhtaseb, A. H., Ihara, I., & Rooney, D. W. (2024). Optimizing biodiesel production from waste with computational chemistry, machine learning and policy insights: A review. *Environmental Chemistry Letters*, *22*(3), 1005–1071. https://doi.org/10.1007/s10311-024-01700-y

Ren, Y., Lv, B., & Ran, Z. (2025). Application of computational fluid dynamics optimized biomimetic microchannel liquid-cooled plates in battery thermal management systems. *Journal of Applied Fluid Mechanics*, *19*(2). https://doi.org/10.47176/jafm.19.2.3810

Rohaizan, M. H. K. M., Sidik, N. A. C., & Shameli, K. (2024). Numerical analysis of heat transfer in microchannel heat sink using flow disruption. *Journal of Advanced Research Design*, *106*(1), 1–14. https://doi.org/10.37934/ard.106.1.114

Sandoval, M. A., Fuentes, R., Walsh, F. C., Nava, J. L., & De León, C. P. (2016). Computational fluid dynamics simulations of single-phase flow in a filter-press flow reactor having a stack of three cells. *Electrochimica Acta*, *216*, 490–498. https://doi.org/10.1016/j.electacta.2016.09.045

Widyaparaga, A., & Pranowo. (2013). Simulation of conjugate convective-conductive heat transfer in a microchannel within the slip regime using GPU accelerated lattice Boltzmann method. In *Proceedings of the ASME 11th International Conference on Nanochannels, Microchannels, and Minichannels (ICNMM2013)* (Paper V001T12A009). https://doi.org/10.1115/ICNMM2013-73133